MODELLING OF CAVITATION IN LARGE SCALE DIESEL INJECTOR NOZZLES

M. Gavaises[1] and E. Giannadakis[2]

[1]City University London, Northampton Square, EC1V 0HB, London
[2]Imperial College London, Exhibition Road, SW7 2BX, London

ABSTRACT

A new Eulerian-Lagrangian cavitation model incorporating a novel approach accounting for bubble motion in Eulerian grids with cell size comparable to that of the cavitating bubbles is validated against experimental data obtained in a multi-hole mini sac-type large-scale diesel multi-hole nozzle replica. The model incorporates many of the fundamental physical processes assumed to take place in cavitating flows. These include bubble formation through nucleation, momentum exchange between the bubbly and the carrier liquid phases, bubble growth and collapse due to non-linear dynamics, bubble turbulent dispersion and bubble turbulent/hydrodynamic break-up. The effect of bubble-to-bubble interaction on momentum exchange and during bubble growth/collapse is also considered. By incorporating many stochastic procedures the model enables the simulation of a fully transient behaviour, even under steady state boundary conditions. Extensive comparison between model predictions and experimental data takes place; those include two-phase cavitating flow images as well as detailed LDV measurements of the flow field. The model predictions show reasonable agreement with the experimentally measured cavitating flow structures.

INTRODUCTION

The performance and exhaust emissions of direct-injection Diesel engines are strongly affected by the nozzle flow exit conditions, which control the atomization process of the injected fuel [1]. Under most operating conditions cavitation is occurring inside the injector nozzle, due to the large pressure drop and the very high fuel velocities encountered. Experimental studies of the flow inside large-scale and real-size nozzle geometries have revealed the complexity of the structures formed over a wide range of operating conditions which correspond to the formation of various cavitation regimes [2-4].

Various numerical cavitation models have recently appeared in the open literature [5-9] employing different assumptions and methodologies. Most models are based on the assumption that cavitation is a mechanically driven phenomenon initiated by the presence of cavitation nuclei inside the bulk of the liquid, which grow to become bubbles in the areas where the local pressure falls below the vapour pressure of the fuel. Then, as observed experimentally, these bubbles form more complex cavitation structures as they further grow and coalesce while moving inside the flow field.

In this paper a recently developed cavitation model is presented and validated against experimental data obtained in a 20x 6-hole large-scale transparent nozzle replica. The well-known Eulerian-Lagrangian methodology is adopted here and it has been combined with the above physical assumption of cavitation inception and development. However, it has been implemented in such a way that allows for bubbles-parcels having volume comparable to that of the volume of the Eulerian cells of the continuous phase to be numerically considered. At the same time, the stochastic nature of the phenomenon is taken into account and detailed physical sub-processes usually neglected are incorporated into the model. In the following sections the model is presented, and results are described and compared with experimental data.

MODEL DESCRIPTION

Flow Solver

The continuous phase flow solver (GFS code) solves numerically in a Eulerian frame of reference the typical conservation equations of incompressible flow, taking into account the effect of the dispersed phase volume fraction and the momentum exchange source term between the two-phases. For the calculation of the dispersed phase volume fraction, a methodology has been developed allowing for the effect of bubbles larger than the occupying cell to be taken into account with sufficient accuracy. This is done by scanning all the cells in the vicinity of the bubble and by calculating a weighted volume contribution to all these cells (Figure 1a). The model also accounts for the presence of wall boundaries on the bubble location, growth and volume distribution, which otherwise may give completely unphysical results, as can be seen in Figure 1b. Additionally, due to the much smaller time step required for the integration of the bubble dynamics phenomena compared to that of the continuous carrier phase, the void fraction contribution of every bubble as it travels through the numerical cells is calculated

by considering its residence time within each cell. It has to be mentioned that in the continuity equation there is no mass source term appearing because the latent mass arising from bubble growth and collapse is negligible, due to the large density ratio. The momentum source term is evaluated by taking into account the effect of contact forces exerted upon the bubbles. Finally, additional to the aforementioned conservation equations, a conventional *k-ε* model is used to simulate the effects of turbulence. A demonstration of the bubble-parcel structure as calculated with the new Lagrangian methodology is shown in Figure 1c.

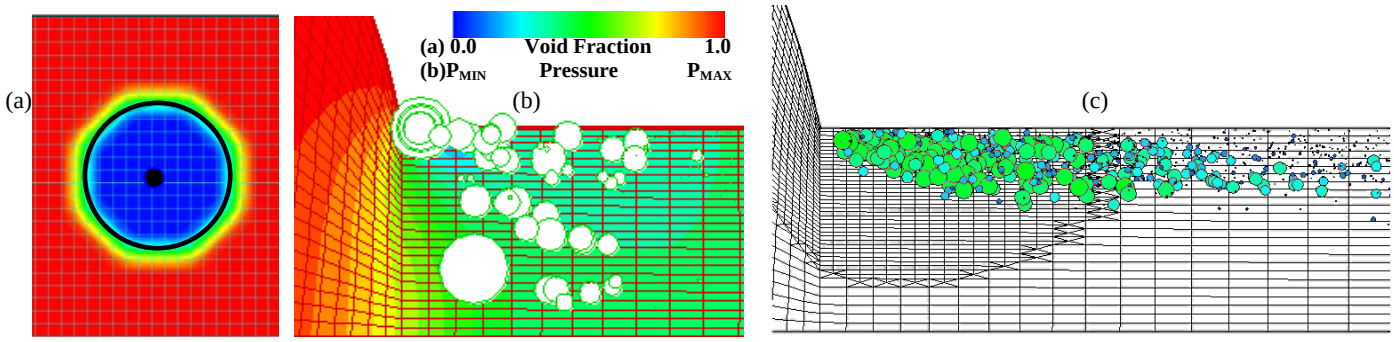

Fig. 1 (a) Demonstration of the bubble-cell common volume, as calculated by the model, (b) Demonstration of the unphysical bubble-parcel characteristics relative to the numerical grid realised in cavitating flows, and (c) bubbly flow image with the new model.

Cavitation Model

Cavitation is initiated by cavitation nuclei, which subsequently grow into bubbles. These bubbles undergo various physical processes, which are taken into account in a stochastic Monte-Carlo approximation. As part of the Lagrangian approximation, bubble parcels are used to simulate the whole population of actual bubbles. These parcels are assumed to contain a number of non-interacting bubbles, which have the same size and velocity and experience the same physical processes. The size of the nuclei is sampled from an assumed pdf. Various distribution functions have been examined; in the one finally adopted, two weighting number densities and two bubble diameters are required as input. The two diameters represent the limiting values of the produced nuclei sizes, while the number densities represent a weighted relative probability between the two. This form resembles measured nuclei number density distributions [10]. The location of the nuclei is determined through another random process. Once the pressure of the liquid falls below its vapour pressure, the volume under tension is identified, and the most probable locations for bubble nuclei formation are calculated randomly by sampling from a distribution function which considers the current bubble volume fraction, the volume and the non-dimensional tension of each Eulerian grid cell. The final input required is the volume fraction of the volume under tension, which is converted into cavitation nuclei; this has a very important effect on the performance of the model. The above inputs define the number of bubble nuclei present in the flow prior to cavitation development. Having determined the size pdf, the average size of a bubble nuclei can be calculated. Given that the total volume of the nuclei is decided as a fraction of the liquid volume under tension the number of nuclei is then calculated by a division of total volume of nuclei by the volume of the average single nuclei. The combination of inputs is such that produces nuclei numbers that match those usually encountered in other bubble-based cavitation models [6,9,11], namely in the range of $10^{12} \sim 10^{15}$ nuclei/m^3. It should be noted that due to the non-linearity of the model, cavitation intensity is not linearly dependent on the predefined total nuclei volume. From various numerical tests it has been concluded that a fraction of the liquid volume under tension (negative pressure) in the range of 0.05~0.5% assigned to the total initial bubble nuclei volume is sufficient to simulate most injector nozzle cavitating flows.

The bubble velocity is calculated according to Newton's second law. The forces arising from the bubbles' interaction with the continuous phase are assessed, and the new velocity for each bubble is calculated. Since the momentum of the bubble itself is negligible, due to the very low mass content, its movement arises from the added mass effect and the acceleration/deceleration of the surrounding liquid. From this perspective, the sum of the forces acting upon the bubble should be zero. The model accounts for the drag, added mass, pressure gradient and lift forces. Buoyancy (also known as Archimedes force) is neglected due to the order of magnitude difference that exists with the rest of the forces for the specific application in diesel injector holes. Furthermore, Basset force is also not considered since bubbles are introduced with no relative velocity with the surrounding liquid and, thus the history force effect has been estimated to be negligible. After having calculated all the forces acting upon the bubbles, the momentum source term needed for the two-way coupling between the Eulerian and Lagrangian phases can then be calculated. In this term only the effect of contact forces is taken into account.

The effect of turbulence on the motion of bubbles is taken into account with a simple dispersion model, adopted from the literature [12]. A random fluctuating velocity is sampled assuming a Gaussian probability distribution function with standard deviation depending on the local liquid turbulence, $\sqrt{2k/3}$. This fluctuating velocity component is added to the mean liquid velocity and through the momentum equation of each bubble the effect of turbulent diffusion is taken into account. In the absence of any reliable model for such a high-speed flow and taking into account that small bubbles are expected to follow faithfully the liquid turbulence, the eddy crossing trajectory effect has been neglected.

Following the assumptions of classical bubble dynamics, the response of a bubble to its variable surrounding pressure field is calculated by integrating the classical Rayleigh-Plesset [13,14] equation. In this approach the effects of local turbulence, relative velocity and surrounding bubbles have all been included. Furthermore, a polytropic coefficient is used which, depending on the bubble wall velocity, switches between adiabatic and isothermal behaviour within the bubble [15].

Due to their motion within the liquid, bubbles deform as a consequence of the shear forces exerted upon them. The origin of these shear forces is local turbulence and the relative velocity of the bubble to that of the liquid flowing around the bubble; both mechanisms are taken into account in the current model. Turbulence induced bubble break-up is included by using the model proposed in [16]. According to the magnitude of the local turbulent kinetic energy dissipation, break-up can occur and in this case the resulting size of the daughter bubbles is generated by the pdf proposed in [17]. Regarding relative velocity induced break-up, a simple criterion based on the Weber number of each bubble is used. In both cases of bubble break-up (turbulence and relative velocity induced) only binary break-up is allowed, which dictates that only two daughter bubbles are produced. It has to be mentioned that for the test cases to be presented here, bubble break-up is relatively less important compared to the other physical processes considered.

RESULTS AND DISCUSSION

Nozzle flow structure and comparison with CCD images

In this section selected results from the model prediction inside a six-hole large-scale nozzle replica are described. For this nozzle model extensive experimental data have been published including CCD and high-speed images of the cavitating flow [18] as well as LDV measurements [19] of the liquid mean and rms velocities under cavitating conditions. The hole diameter was 3.5mm, which corresponds to a diameter of 0.175mm in the real size nozzle. The needle lift was kept constant to its maximum value of 6.0mm (0.3mm in the real size injector), while the nozzle geometry was based on a Bosch mini sac-type nozzle. The working fluid was a mixture of hydrocarbons having the same refractive index of 1.49 to that of the Perspex nozzle at room temperature; Table 1 summarises the various conditions investigated.

Table 1: Operating conditions investigated [Needle lift 6.0mm]

Cavitation Number (CN)	Reynolds Number (Re)	P_{INJ} (bar)	P_{BACK} (bar)	Hole Flow Rate (l/s)	Mean velocity (m/s)
0.45	21000	1.80	1.27	0.095	9.85
1.09	30200	2.40	1.20	0.136	14.15
4.57	39500	4.00	0.80	0.178	18.50

The numerical grid constructed was consisting of ~10^5cells while approximately 10^4 bubble parcels were present inside the injection hole at every time step. The total computational (CPU) time of the cavitation runs (including both the continuous phase solver and the Lagrangian bubble parcels) was of the order of 1h per time step on a Pentium 4 running with a 2.8GHz processor. As mentioned, although steady pressure (or flow rate) boundary conditions have been employed, the flow itself is transient. This is mainly due to the formation, growth and transport of the cavitation bubbles, which, in turn, affect the pressure and velocity distribution inside the injection hole. Therefore, around 100 continuous phase time steps of $5 \cdot 10^{-4}$s each were required in order to get predictions that can be compared with LDV measurements. The time step for the tracking of the cavitation bubbles was $2.5 \cdot 10^{-6}$s while an even smaller but adaptive time step with a minimum value of 10^{-12}s was used for the integration of the Rayleigh-Plesset equation of bubble dynamics. As a general trend, the cavitation model predicts a reduction of the nozzle flow rate with increasing cavitation intensity, which has been found to agree reasonably with the experimental data. At the same time it predicts a pressure recovery from the negative values calculated by the single-phase flow solver in the cavitation region which, results to an overall reduction in the cavitation tension zone, as described in more detail in [19].

In order to be able to extrapolate the conclusions of the large-scale nozzle flow investigation to that of the real-size nozzle, dynamic flow similarity based both on the Reynolds and cavitation numbers has been employed. The cavitation number, defined here as $CN = (P_{INJ}-P_{BACK})/(P_{BACK}-P_{VAPOUR})$, has been selected as the main dimensionless parameter characterising the various flow regimes formed inside the injection hole. It has been shown that this parameter can also define the threshold between single-phase flow and cavitation inception. For this particular nozzle investigated, cavitation was initiating for cavitation numbers around 0.9. Initially, the so-called incipient cavitation regime is realised, mainly consisting of dispersed bubbles formed at the low-pressure region present to the entrance of the injection holes. For this flow regime, flow images and LDV measurements have been obtained for CN=1.09. With increasing cavitation number the bubbles become larger and more vapour volume is formed inside the hole until a point is reached when an almost stable canopy-shaped vapour pocket is formed at the top of the injection hole; further down the hole is occupied by a dense bubble cloud. For this fully developed cavitating flow regime, CCD-based images obtained at CN=4.57 from three different views are shown in Figure 2 together with the corresponding model predictions for the void fraction distribution. As can be seen, the highest amount of vapour is attached to the top of the hole while it diffuses towards the exit. At the same time, the predictions show a two-vortex structure formed on the upper part of the hole. Those vortices originate from the hole inlet, as clearly shown in Figure 3, and extend up to the hole exit. Representative bubble-parcels, coloured according to their size are also plotted together with their velocity vector, scaled to velocity magnitude. Additionally the streamlines inside the sac volume are also plotted and coloured according to the w-velocity component of the liquid, which is in the direction of the nozzle axis. As clear, the flow entering into the sac volume is forced to turn sharply inside the sac volume, reverse its direction and enter into the injection hole from the bottom side of the hole-entrance. As a result, the flow inside the sac volume is always rotating and highly unsteady, as model predictions have confirmed. Another point of interest is related to the extent of the recirculation zone formed to the top of the hole-entrance. As can be seen in Figure 3, at this location a double-vortex structure is formed with relatively higher intensity in the lower cavitation number case. This is mainly due to the fact that with

increasing cavitation intensity, the recirculation zone at the hole-entrance is suppressed, as LDV measurements obtained at this location have also confirmed [20].

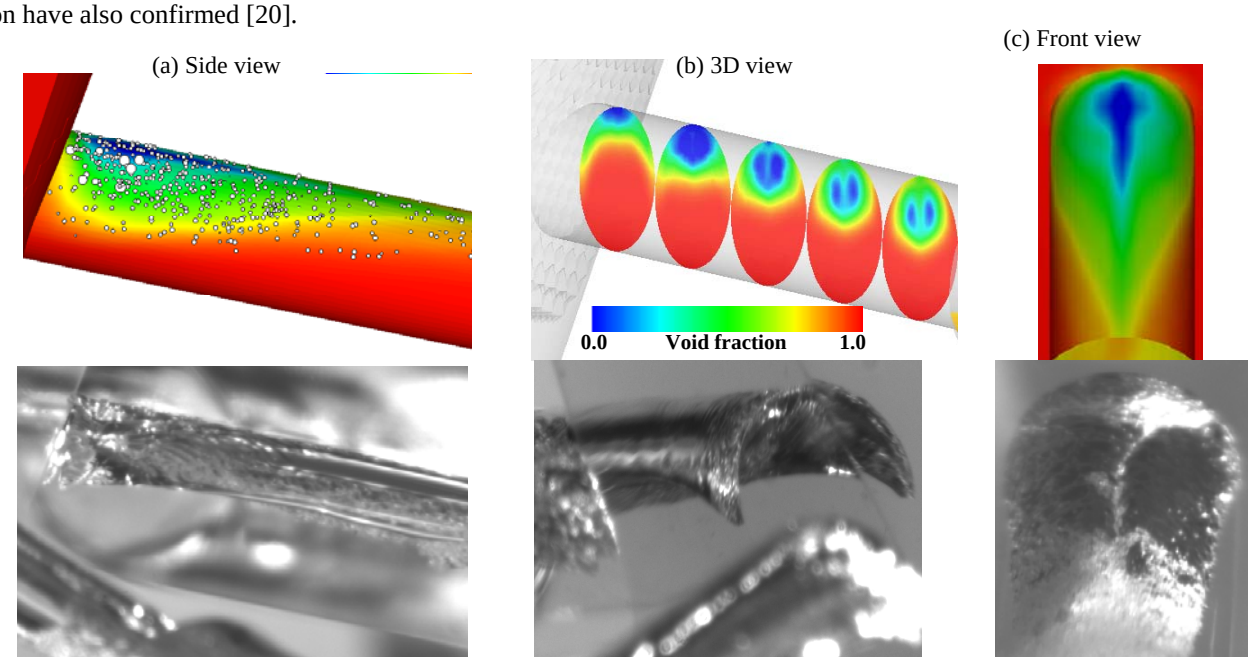

Fig. 2 Comparison between model predictions of the vapour void fraction with cavitating flow images at CN=4.57 (fully developed cavitation). The canopy-shaped vapour distribution at the entrance to the injection hole is shown in the middle image. Model predictions for the void fraction show the two vortices formed at the top of the injection hole.

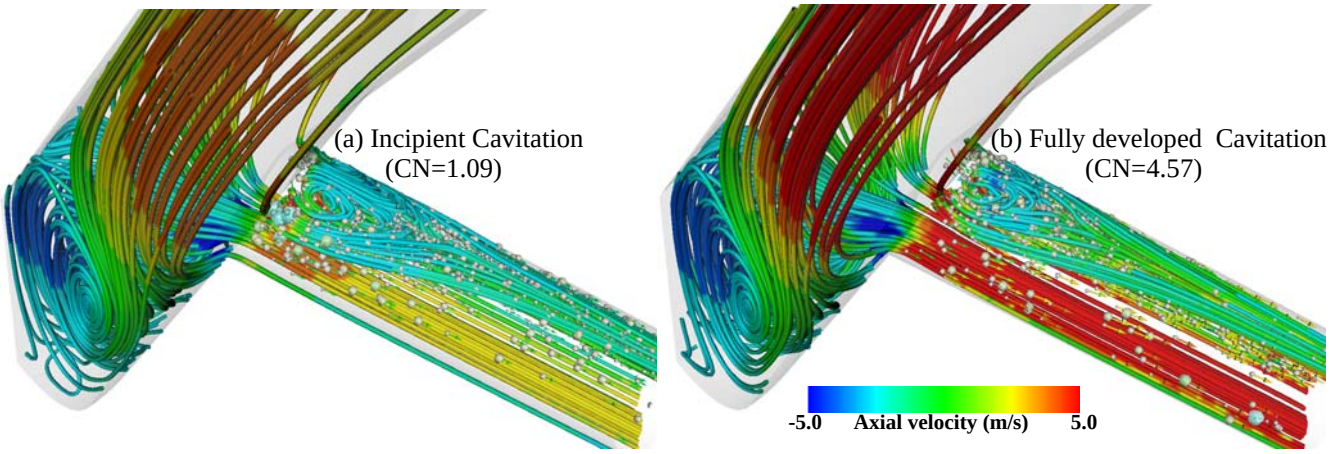

Fig. 3 Tilted side view of the predicted flow-path lines inside the sac volume and the injection hole at two different cavitation numbers of (a) 1.09 and (b) 4.57, together with representative bubble-parcels. The rotating flow structure inside the sac volume is clear for both cases. The recirculation zone formed at the hole-entrance is larger in the case of lower cavitation number.

Comparison against LDV measurements

In this section of the paper the model results are compared with LDV measurements for the conditions of Table 1. Initially comparison takes place for the non-cavitating case of CN=0.45. Mean and rms velocity measurements and calculations are shown in Figures 4 and 5 on three vertical lines located on the symmetry plane of the nozzle. The measurement locations relative to the hole-length have been selected to be close to the hole inlet, at middle distance of the hole length and at its exit, therefore covering the whole area of interest. For all three conditions investigated here, the velocity profile is normalised with the mean injection velocity of each particular case, thus allowing direct comparison between them and also revealing the effect of cavitation on the measured and calculated velocity distribution inside the injection hole.

In the case of single-phase flow shown in Figure 4a for the mean velocity, the model predictions seem to follow the same trend as the LDV measurements although they underestimate the extend as well as the intensity of the recirculation zone formed at the top of the hole entrance. This is mainly due to the grid spacing as well as to the selection of the model of turbulence used, and its solution would require much more dense grids and computationally expensive turbulence models to be employed. Therefore, the accuracy obtained is considered satisfactory for continuing to the comparison with the cavitating cases.

Figures 4b and 4c show the comparison between measurements and predictions of the mean velocity for the incipient and the fully developed cavitating cases. At this time, model predictions are shown for 12time instances, spaced by 10 successive computational time steps between them. The transient nature of the model is clearly realised. Overall, the flow accelerates towards the exit of the nozzle hole due to the production of the vapour, which leaves less space for the liquid to flow. This effect, clearly

shown in the experimental data is well represented by the model. The overall increase of the velocity and the corresponding hole-exit area blockage has been calculated to be around 10 to 15%. Another effect also evident is the smaller velocity of the liquid at the hole-inlet with increasing cavitation number. As already mentioned, with increasing cavitation number the recirculation zone formed at the hole-inlet is suppressed. In that case model predictions are very close to the measurements relative to the non-cavitating case.

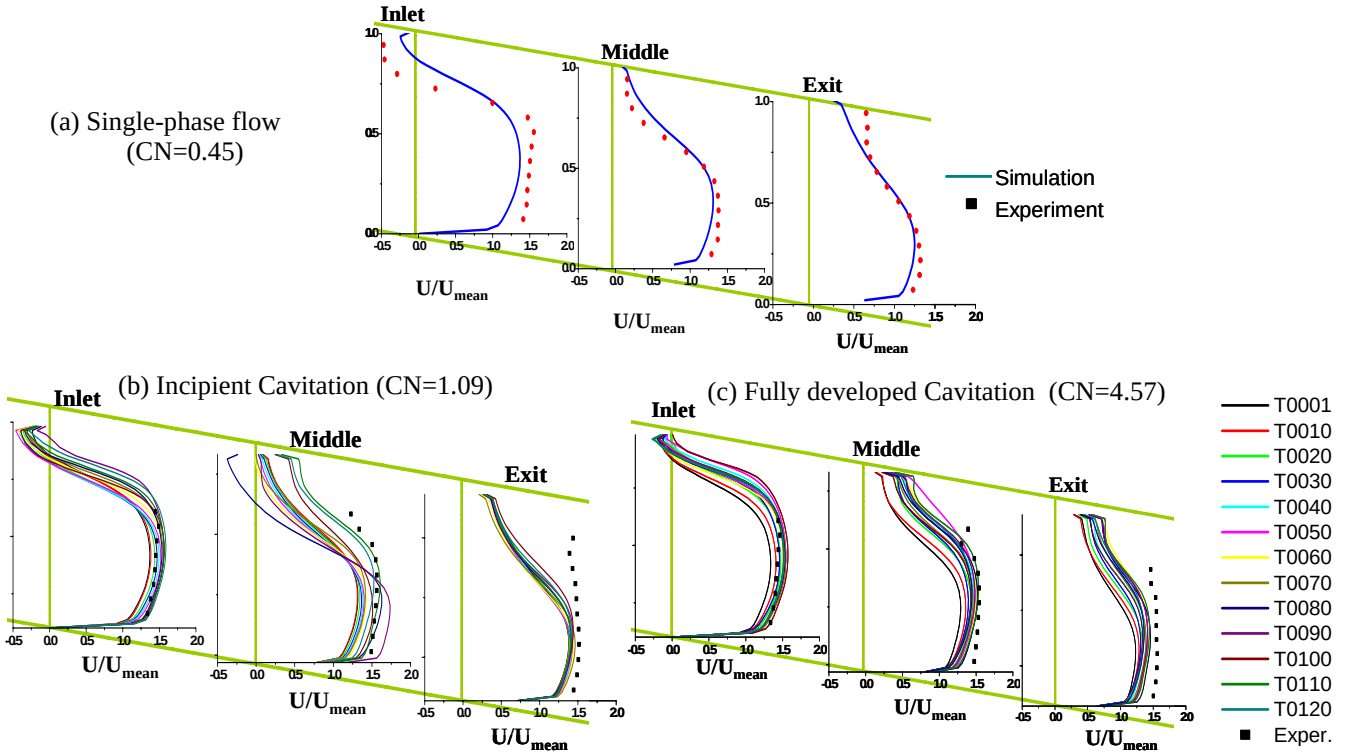

Fig. 4 Comparison between LDV measurements and model predictions for the mean velocity at three cross sections located at the entrance, middle distance and exit of the injection hole both for non-cavitating and cavitating flow conditions. Model predictions are plotted at selected time steps, also revealing the transient behaviour of the flow (a) single-phase, (b) incipient cavitation and (c) fully-developed cavitation.

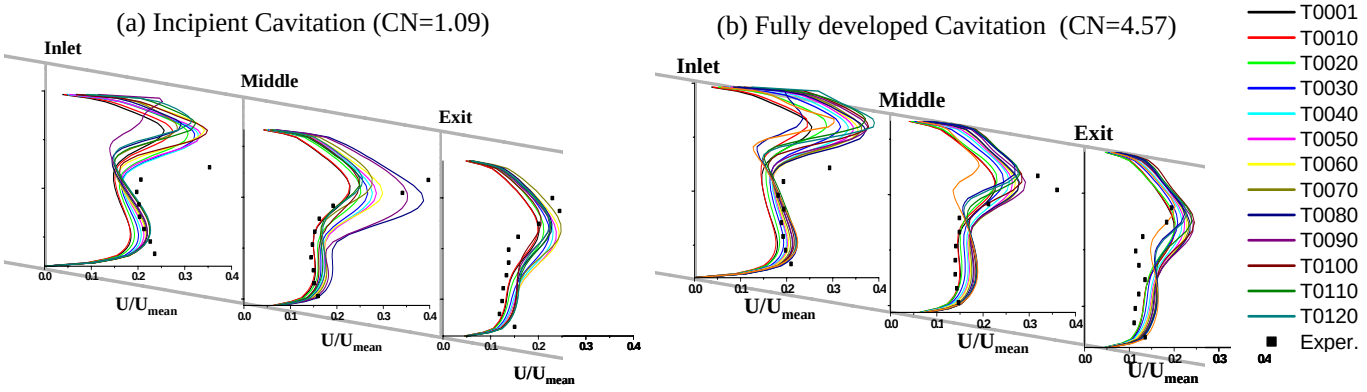

Fig. 5 Comparison between LDV measurements and model predictions for the rms (turbulent) velocity at three cross sections located at the entrance, middle distance and exit of the injection hole. Model predictions are compared at selected time steps for the (a) with the incipient cavitation case and (b) fully developed cavitation case, revealing the transient behaviour of the flow.

The last Figure 5 shows the comparison between the measured and the predicted rms velocity again at the same measurement planes. The model captures the order of magnitude of the rms velocity, which is around 20 to 25% of the mean velocity. At the same time, its spatial distribution is reasonably well represented, although differences exist in the area of flow reattachment. In this area, both experimental data and model predictions show that turbulent levels almost double relative to those of the pure liquid flow flowing below the highly cavitating zone found at the top part of the injection hole. Overall, it seems that under cavitating conditions the turbulence levels increase mainly near the hole-inlet. However, this increase is relatively smaller towards the hole-exit.

CONCLUDING REMARKS

A new cavitation model has been developed, based on a Eulerian-Lagrangian approach, which assumes that cavitation consists of discrete bubbles but which can have volume larger than that of the computational cells. Simulations of the cavitating flow in a large-scale transparent 6-hole diesel nozzle replica have been performed for single-phase, incipient cavitation and fully developed cavitation regimes. The incorporation of many stochastic procedures in the model allows a fully transient behaviour, even under steady-state boundary conditions. Model predictions were compared against CCD images of the cavitation inside the injection hole and also with LDV measurements of the mean and rms velocity at different planes located at the inlet, middle and exit of the injection hole. A drop in the nozzle flow rate relative to the single phase value is also predicted by the model, which is consistent with the drop in the discharge-coefficient observed in nozzles under cavitating conditions. Finally, LDV mean and rms velocity measurements show an increase of the average velocity of the liquid emerging from the nozzle, which is also predicted by the model.

ACKNOWLEDGEMENTS

The authors would like to acknowledge the contribution of Mr H.Roth who was responsible for the experimental results and the financial support of the EU I-Level research programme supporting the development of the cavitation model. Also the contribution of Toyota Motor Engineering and Manufacturing Europe (TMEM) is deeply acknowledged.

REFERENCES

1. Heywood J.B., *Internal Combustion Engine Fundamentals*, McGraw-Hill, New York, 1989.
2. Arcoumanis C., Badami M., H. Flora and Gavaises M., Cavitation in Real-Size Multi-Hole Diesel Injector Nozzles, *SAE Paper 2000-01-1249*, 2000.
3. Chaves H., Knapp M., Kubitzek A., Obermeier F. and Schneider T., Experimental Study of Cavitation in the Nozzle Hole of Diesel Injectors Using Transparent Nozzles, *SAE Paper 950290*, 1995.
4. Soteriou C., Andrews R., and Smith M., Direct Injection Diesel Sprays and the Effect of Cavitation and Hydraulic Flip on Atomization, *SAE Paper 950080*, 1995.
5. Avva R.K. Singhal A. and Gibson D.H., An Enthalpy Based Model of Cavitation, *ASME FED*, vol. 226, pp 63-70, 1995.
6. Grogger H. and Alajbegovic A., Calculation of the Cavitating Flow in Venturi Geometries using Two-Fluid Model, *FEDSM98-5295, ASME Fluids Engineering Summer Meeting*, 1998.
7. Marcer R., Le Cottier P., Chaves H., Argueyolles B., Habchi C. and Barbeau B., A Validated Numerical Simulation of Diesel Injector Flow Using a VOF Method, *SAE Paper 2000-01-2932*, 2000.
8. Schmidt D.P., Rutland C.J. and Corradini M.L., A Numerical Study of Cavitating Flow Through Various Nozzle Shapes, *SAE Paper 971597*, 1997.
9. Yuan W., Sauer J. and Schnerr G.H., Modeling of unsteady cavitating flows in fuel injection nozzles, *Proceedings of ILASS 2000,* Darmstadt, 2000.
10. Meyer R.S., Billet M.L. and Holl J.W., Freestream Nuclei and Traveling-Bubble Cavitation, *Journal of Fluids Engineering-Transactions of the ASME*, vol 114, issue 4, pp 672-679, 1992.
11. Kubota A., Kato H., and Yamaguchi H., A New Modeling of Cavitating Flows - a Numerical Study of Unsteady Cavitation on a Hydrofoil Section, *Journal of Fluid Mechanics*, vol 240, pp 59-96, 1992.
12. Farrell K.J., Eulerian/Lagrangian Analysis for the Prediction of Cavitation Inception, *Journal of Fluids Engineering-Transactions of the ASME*, vol 125, issue 1, pp. 46-52, 2003.
13. Brennen C.E., *Cavitation and Bubble Dynamics*, Oxford University Press, 1995.
14. Plesset M.S. and Prosperetti A., Bubble Dynamics and Cavitation, *Annual Review of Fluid Mechanics*, vol 9, p. 145-185, 1977.
15. Moss W.C., Levantin J.L. and A.J. Szeri, A New Damping Mechanism in Strongly Collapsing Bubbles, *Proceedings of the Royal Society of London A*, vol 456, issue 2004, pp 2983-2994, 2000.
16. Martínez-Bazán C., Montañés J.L. and Lasheras J.C., On the breakup of an air bubble injected into a fully developed turbulent flow - Part 1: Breakup frequency, *Journal of Fluid Mechanics*, vol 401, pp 157-182, 1999.
17. Martínez-Bazán C., Montañés J.L. and Lasheras J.C., On the breakup of an air bubble injected into a fully developed turbulent flow - Part 2: Size PDF of the resulting daughter bubbles, *Journal of Fluid Mechanics*, vol 401, pp 183-207, 1999.
18. Afzal H., Arcoumanis C. Gavaises M., and Kampanis N., Internal flow in Diesel injector nozzles: modelling and experiments, *Proc. 3rd IMeCHE International Seminar on Fuel Injection Systems*, London, 1-2 December, 1999.
19. Giannadakis E., Gavaises M., Roth H. and Arcoumanis C. "Cavitation Modelling based in Single-hole injector based on Eulerian-Lagrangian Approach", accepted for publication in THIESEL 2004 Conference on Thermo- and Fluid-Dynamic Processes in Diesel Engines, Valencia, September 10-13, 2004
20. Roth H., Gavaises M. and Arcoumanis C., Cavitation Initiation, Its Development and Link with Flow Turbulence in Diesel Injector Nozzles, *SAE Paper 2002-01-0214*, SAE Transactions, 2002.